

Hydrodynamics Characterization of the Impact of Free-Moving Particles in an Air-Lift Membrane Bioreactor

Naila Bouayed, Anthony Cavalier, Christine Lafforgue, Nicolas Dietrich, Chung-Hak H Lee, Christelle Guigui

▶ **To cite this version:**

Naila Bouayed, Anthony Cavalier, Christine Lafforgue, Nicolas Dietrich, Chung-Hak H Lee, et al.. Hydrodynamics Characterization of the Impact of Free-Moving Particles in an Air-Lift Membrane Bioreactor. Industrial and engineering chemistry research, 2020, pp.7943-7954. 10.1021/acs.iecr.9b06749 . hal-02542064

HAL Id: hal-02542064

https://hal.insa-toulouse.fr/hal-02542064

Submitted on 14 Apr 2020

HAL is a multi-disciplinary open access archive for the deposit and dissemination of scientific research documents, whether they are published or not. The documents may come from teaching and research institutions in France or abroad, or from public or private research centers.

L'archive ouverte pluridisciplinaire **HAL**, est destinée au dépôt et à la diffusion de documents scientifiques de niveau recherche, publiés ou non, émanant des établissements d'enseignement et de recherche français ou étrangers, des laboratoires publics ou privés.

HYDRODYNAMICS CHARACTERIZATION OF THE IMPACT OF FREE MOVING PARTICLES IN AN AIR-LIFT MEMBRANE BIOREACTOR

N. BOUAYED[1], A. CAVALIER[1], C. LAFFORGUE[1], N. DIETRICH[1], C.H. LEE[2] & C. GUIGUI[1,*]

1. Toulouse Biotechnology Institute (TBI), Université de Toulouse, CNRS, INRAE, INSA, Toulouse, France
2. School of Chemical and Biological Engineering, Seoul National University, Seoul 151-744, Republic of Korea

* To whom correspondence should be addressed.
Tel.: +33(0)5 61 55 97 90 ; Fax: +33 (0)5 61 55 97 60 ; E-mail: Christelle.Guigui@insa-toulouse.fr

Abstract

Membrane fouling is one of the most investigated topics in the field of membrane processes because it is the main weakness that prevents membrane bioreactors (MBRs) from being widely applied. With a view to reducing membrane fouling, all the phenomena involved in the operation are worth understanding through a fine-tuned and deep examination. In the present paper, the study focused on the hydrodynamics in an air-lift MBR with a flat sheet membrane, taking into account the application of a specific method for biofouling mitigation adding free moving particles in addition of bubbles injection. The application of this technique creates a complex three-phase gas-liquid-solid contactor in the MBR in terms of hydrodynamics. Therefore, the main objective of this work was to properly characterize, using a Particle Image Velocimetry (PIV) technique, such a system in order to clarify the potential effect of the addition of free moving solid particle on the hydrodynamics and the performances of the MBR. Three different shape of particle have been tested: beads, hollow cylinders and flat sheets. Local hydrodynamic parameters, such as the liquid velocity, the liquid shear stress, or the bubble sizes and velocities were analyzed with and without the presence of solid particles. Specific conclusions are drawn to help future user of this antifouling technique to optimize the design for the solid particle.

Key-words: Membranes Bioreactors (MBRs), Air-Lift Reactors (ALRs), hydrodynamics, Particle Image Velocimetry, gas-liquid-solid.

1. INTRODUCTION

Membrane bioreactor (MBR) is the combination of a membrane process like microfiltration or ultrafiltration with a biological wastewater treatment process, the activated sludge process [1]. Over the past two decades, MBRs emerged as a highly potent process in advanced Wastewater Treatment (WWT) owing to their exceptional features. Among all the WWT processes known to date, the innovative MBR technology has been plainly proved to provide excellent effluent quality, total biomass retention, high biomass concentrations, high organic removal efficiency, high organic loading rate and low production of excess sludge. Moreover, the environmental footprint of MBRs has been reported to be low in comparison with conventional processes [2,3]. Furthermore, the compactness and the modularity of MBRs design, added to the aforementioned advantages, have promoted their application to treat both industrial and municipal wastewaters (WW) [4–6]. Yet, the extensive development of MBRs for WWT is still restricted by some remaining weaknesses among which membrane fouling is the most severe one.

Membrane fouling results from the complex combination of several phenomena, such as: deposition and accumulation of solids from the mixed liquor, bacterial growth (also called biofilm), pore clogging, adsorption of secreted products, which lead to the formation of a cake layer onto the membrane surface. Membrane fouling gives rise to an overall reduction in the MBR performance by causing a severe loss of permeability, and thus increase in energy consumption and a heightened need to clean or replace the membrane, which results in a substantial increase in the operating costs. Therefore, in order to mitigate this phenomenon, several cleaning methods have been developed and can be classified into physical, chemical and biological ones.

Among the physical methods, one of the most applied ones is air-sparging that consists in the injection of coarse bubbles for the membrane scouring and this method was proved to be

efficient to reduce membrane fouling owing to the increased shear stress created by the bubbles on the membrane surface. Moreover, when the air-sparging system was implemented between two flat membranes, an Air-Lift Reactor (ALR) is created, the mitigation of membrane fouling was even more efficient owing to the higher cross flow velocity induced [7–11].

Another method proposed for fouling mitigation belongs to the biological methods and is related to: Quorum Quenching (QQ). QQ consists in the disruption of Quorum Sensing (QS), a cell-to-cell communication mechanism enabling biomass from MBRs to harmonize their behavior for the production of biofilm. Since biofilm is recognized as a major part of the cake layer formed on the membrane surface and responsible of the fouling, QQ was developed as a preventive method for biofouling control in MBRs. The principle of QQ is to degrade, via the addition of an enzyme or an enzyme-producing strain, the signal molecules (AHLs) thanks to which the major part of bacteria in MBRs communicate. Recent works have shown that when QQ bacteria were immobilized into small capsules and implemented in MBRs, the biofouling phenomenon was considerably delayed [12]. For more information on the QQ mechanism and its application to MBRs, the reader is invited to consult these reviews [13,14,1,15]).

In the literature, the first media that has been reported is a microbial vessel composed of hollow fibers inside which the QQ bacteria (*Rhodococcus* sp. BH4 or *Pseudomonas* sp. 1A1) are captured (Jahangir et al., 2012; Oh et al., 2012, 2013). The microbial vessel is usually held in a fixed place in the MBR, in opposition to the other Solid media that have been further developed such as QQ beads which are free-moving suspended particles containing the same QQ bacteria. Recently, different shapes such as hollow cylinders or sheets have been developed as Solid media [16–18]. In order to study the behavior of these solid media under different operating conditions in the MBR, and their influence on the overall hydrodynamics, the different Solid media were introduced in the lab-scale MBR. In the case of the free-

moving Solid media (beads, HC and sheets) the number of suspended objects can be a key parameter, since it is directly correlated with the concentration of QQ bacteria in the MBR. In addition, these objects are also expected to have a mechanical effect on the membrane, thus, the greater their number is, the more pronounced can be the physical washing effect. Fluidization is also a key-phenomenon since it ensures the continuous circulation of Solid media in the reactor and thus, it increases the probability of contact and thereby to exert a mechanical washing effect on the membrane, which was proved to be involved in the biofouling mitigation [19–23]. These findings were in perfect accordance with other studies that widely demonstrated the effective reduction of fouling in MBRs by the addition of solid particles, such as synthetic micro-particles [24], granular activated carbon [25], or other granular scouring agents (reviewed by [26]), not only by the sole membrane scouring but also by inducing structural modifications of the microbial flocs and the cake layer [27]. Besides, these suspended particles can also play an important role in the hydrodynamics of the reactor which is a key-factor for the overall MBR performance. Therefore, the optimization of the Solid media fluidization is of great interest and was here addressed by taking into account important parameters such as the hydrodynamics (air flowrate), the ALMBR geometry (riser width) and the Solid media (quantity and shape).

Hence, the objective of the present work is to study the hydrodynamics of an MBR coupling the two aforementioned techniques: Quorum Quenching particles and Air-Lift Reactor with flat sheet membrane in pure water with inert QQ media. This results in a complex three-phase bioreactor for which the hydrodynamics behavior can be of critical importance to optimize the performance of the system.

2. MATERIAL AND METHODS

The experiments were carried out in a lab-scale MBR with a total working volume of 18 L, composed of an anoxic tank (5 L) and an aerobic tank (13 L), in a similar way to the one described by another research work and to classical industrial configurations (Figure 1) (Li et al., 2015). The MBR was fed in the anoxic tank, which was stirred, and the overflow dropped into the aerobic membrane tank. A PES flat sheet membrane with a total area of 0.1 m^2 and a pore size of 0.2 µm (Kubota, Japan) was used as a filtration module, and the instantaneous permeate flux was set to 15 L/m^2 h (LMH). A continuous recirculation from the aerobic tank to the anoxic tank was fixed to 4 L/h. The membrane tank was equipped with an air-sparging system consisting in a coarse air bubbles injection through a perforated tube, composed of two rows of seven 2 mm-holes each, and located at the bottom of membrane (Figure 1).

Two baffles were set on both sides of the membrane, creating an air-lift configuration with three separated parts: an aerated part with an upward circulation called the riser in the center, and two non-aerated parts called the down-comer, on both sides. This air-lift configuration generated an external loop for liquid circulation with no gas recirculation in the down-comer part (figure 1). All the operating conditions are gathered in Table 1.

The MBR was operated in model conditions with tap water with a view to studying the hydrodynamics in the membrane tank, given that the upward movement of bubbles prevails by far over the potential settling of particles in real activated sludge (Brannock et al., 2010, 2009; Yan et al., 2015). All experiments were performed at ambient temperature of 293 K.

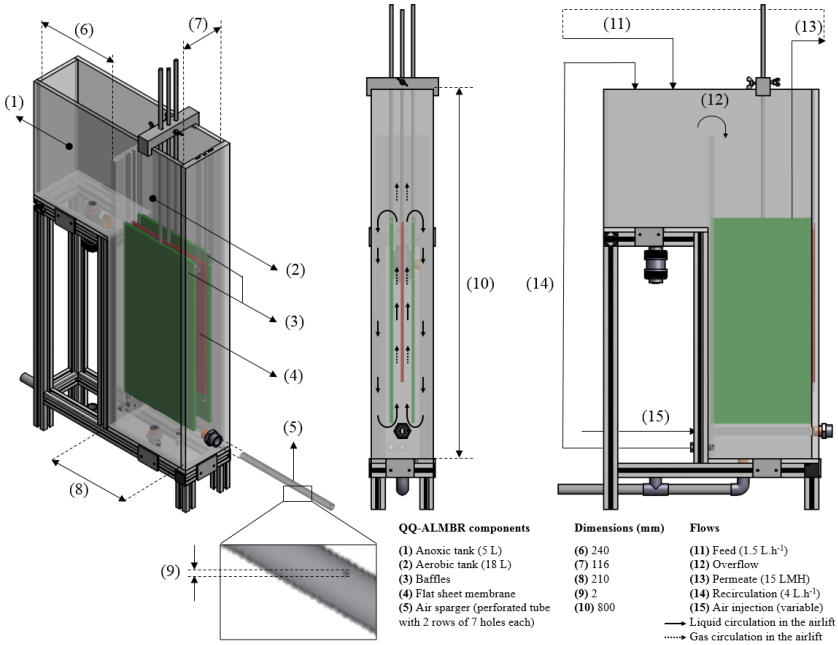


Figure 1 : Diagram of the Quorum Quenching Air-Lift Membrane Bioreactor (QQ-MBR).

Table 1 : Air-lift Membrane Bioreactor (MBR) operating conditions.

Operating conditions	
Air-lift	
Riser width $2D_r$ (mm)	[14 ; 30]
Down-comer width $2D_d$ (mm)	[80 ; 64]
Riser cross sectional area A_r (m²)	[0.00294 ; 0.0063]
Down-comer cross sectional area A_d (m²)	[0.0168 ; 0.01344]
A_r/A_d ratio (-)	[0.175 ; 0.469]
Liquid height (m)	0.585
Membrane	
Type	Flat sheet
Material	PES
Total area (m²)	0.1
Average pore size (µm)	~ 0.2
Bioreactor	
Total working volume (L)	18
Total HRT (h)	12
Temperature (°C)	~ 20 (room temperature)
Filtration flux (LMH)	15
SADm ($Nm^3.h^{-1}.m^2$)	[0.3 ; 0.4 ; 0.75 ; 0.9 ; 1.0]

In order to study the potential influence of quorum quenching particles implementation on the MBR from a hydrodynamic point of view, different vacant particle media (with no bacteria and thus no biological activity) were introduced in the aerobic tank (figure 2). The solid particles used in this study were made of sodium. The production method consisted in dripping a homogeneous liquid alginate suspension (complemented without a bacteria suspension in our case) into a $CaCl_2$ solution to obtain solid particles, with different shapes, as

reported in the literature [17,18,20]. The physical properties of the different media are gathered in Table 2.



Figure 2: Photographs of media used in the study: (a) beads (b) hollow cylinders and (c) sheets.

Table 2 : Physical characteristics of the Solid media.

	Beads	**Hollow cylinders**	**Sheets**
Dimensions (mm)	Diameter: 3.5	Inner diameter: 1.7 Outer diameter: 3.5 Length: 27	Length: 20 Width: 10 Thickness 0.5
Volume (mm^3)	22.5	198.5	100
Surface (mm^2)	38.5	455.8	400
Wet density ($g.cm^{-3}$)	1.074 ± 0.002	1.06 ± 0.01	1.063 ± 0.004
Terminal free-falling velocity (m/s)	0.035 ± 0.002	0.024 ± 0.003	0.011 ± 0.002
Total number of introduced media (-)	2600	298	585

The hydrodynamics of the MBR was studied by determining velocity fields using the Particle Image Velocimetry (PIV) technique. In that purpose, the MBR filled with tap water was seeded with tracer particles (Silver-coated Hollow Glass Spheres (S-HGS), Dantec Dynamics) with a density of 1.4 g/cm^3, a size distribution ranging from 10 to 30 µm and an average diameter of 15 µm. The middle vertical plane of the reactor was illuminated with a laser sheet (Nd:YAG unit laser source, DualPower 200-15, class 4, Dantec Dynamics) and the trajectories of the tracer particles in the liquid flow were captured orthogonally to the laser

sheet in different representative areas of about 55 x 55 mm², with a high speed camera (FlowSense EO 4M, 2048 x 2048 pixels², 20.4 fps, Dantec Dynamics) equipped with a 105 mm lens (Micro-NIKKOR, 105 mm, Nikon) (figure 3). The acquisition was set to 10 pairs of pictures per second for 25 s to obtain an average flow field in the focused region. The time between two pictures was adjusted according to the velocity induced by the air flowrate and ranged from 0.5 to 5 ms. The images were captured and analyzed using the appropriate software (DynamicStudio 2015a) and the average water velocity fields were obtained by cross-correlating the two consecutive pictures of each pair. Finally, the resulting digitalized data were processed using a Matlab program to determine information about the liquid flow.

In order to characterize both of the gas phase and the solid phase, a direct visualization technique was used. The experimental setup consisted in a camera (acA1920 - 155 um, 1920 x 1200 pixels², 164 fps, Basler) with a 105 mm lens (Micro-NIKKOR, 105 mm, Nikon). A backlight panel (Phlox-LedW-BL, 400 x 200 mm², 24 V, 2A, Phlox) was set up against the back of the aerobic tank in order to illuminate the reactor (figure 3). The acquisition of pictures was set to 200 Hz and lasted 15 s. The images were acquired using the appropriate software (pylon Viewer 64-bit) and then processed using a Matlab program to determine the bubble size and velocity[28–31].

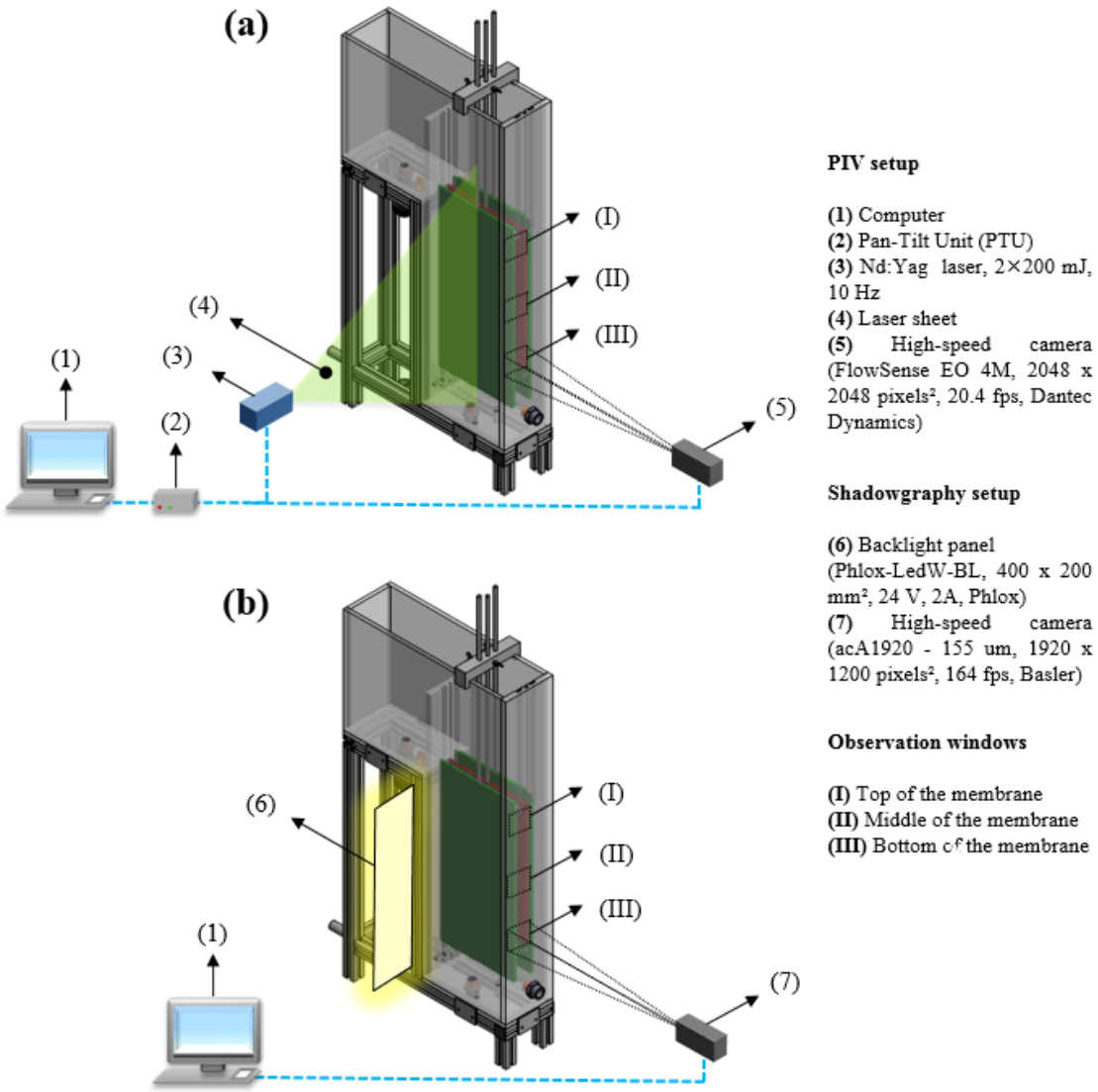


Figure 3 : (a) PIV setup and (b) visualization setup for the hydrodynamics characterization.

Since the measurements were carried out with optical techniques that needed transparent media, all the experiments were conducted with tap water and thus without any biological activity. On the other hand, the PIV requires the addition of tracer particles in a certain concentration that has to be maintained. For these reasons, the MBR was not fed and the permeate flux was totally recycled to the anoxic tank to ensure the continuous operation (figure 1). Also, since both of the recirculation flowrate (4 L/h) and the permeate flux (15 LMH) are relatively low and flow into the anoxic tank (i.e. “far” from the aerobic tank), their effect on the global hydrodynamic behavior was assumed to be negligible. Therefore, the

operating conditions that have been varied were only the ones that can significantly impact the hydrodynamics and the fluidization of the Solid media in the MBR and are explained below.

The first important parameter to study was the volume fraction (% v/v) of Solid media to introduce which is defined as the ratio of their total volume to the total liquid volume of the aerobic tank (13 L). Three different volume fractions were selected according to those reported in the literature were used: 0.06 % v/v (Kim et al., 2013), 0.10 % v/v (Maqbool et al., 2015) and 0.45 % v/v (Kim et al., 2015).

The distance between the membrane and the baffles, also corresponding to the width of half of the riser part (D_r), could be set to two different positions: 15 mm and 7 mm which is the actual distance separating two membrane panels in industrial flat sheet (FS) modules. This is an important parameter to study because it directly represents the space offered for the solid media and the bubbles to upwardly circulate near the membrane.

Another key-parameter to vary was the air flowrate in the air-sparging system. Five different values were chosen based on the literature and ranged from 0.03 to 0.1 Nm^3/h (i.e. 0.3 to 1.0 in terms of Specific Aeration Demand based on the membrane area (SADm) and 30 to 100 Nm^3/m^3 permeate in terms of Specific Aeration Demand based on the permeate volume (SADp), which fits into the range recommended for MBRs systems (10 to 100 Nm^3/m^3 permeate).

Since the camera only allowed the observation of restricted areas (about 55 x 55 mm^2), three representative windows (I, II, III) were defined in the top, the middle, and the bottom of the membrane, respectively (figure 2).

3. RESULTS AND DISCUSSION

3.1 Hydrodynamics in a two phases flow reactor

The PIV technique was used to measure velocity fields in the liquid phase[32,33]. For each operating condition presented, 250 images were recorded, processed, and then digitalized. An example of the obtained raw results by this technique is presented in figure 3 and shows the velocity field in the liquid phase for the observed area. The comparison between the picture (figure 4.a) and the velocity field (figure 4.b) shows that the red areas correspond to the bubbles streaks where higher velocities are induced.

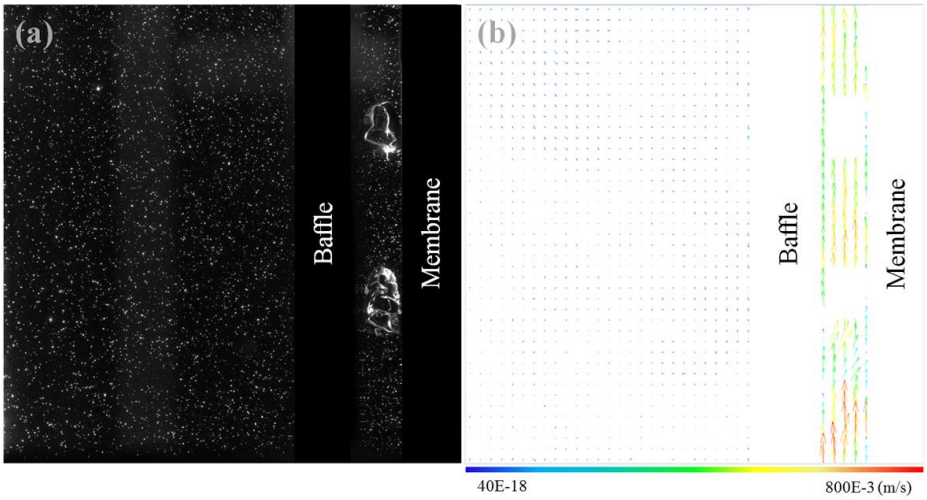


Figure 4 : Example of velocity field (b) from the analysis of a PIV image (a) recorded in the MBR at the top of the membrane (window I), with D_r = 7 mm and under a SADm of 1.0 $Nm^3.h^{-1}.m^2$.

In order to focus on the liquid phase, the possible effect of bubbles on images processing was attenuated by averaging the 250 images to get an average velocity field. For each operating condition, the liquid flow was studied in half of the riser part (the MBR is assumed to be symmetrical about the membrane (figure 1)). In this space, the average vertical and horizontal velocities of the liquid were determined and are presented in figure 5 and figure 6, respectively.

The error bars represent the standard deviation which indicate the dispersion of data. In that case, the analysis of the error bars shows that the greater the air flowrate is, the wider is the

range in which the data points spread out. This means that heterogeneous velocity fields tend to be induced at higher air flowrates, with up to ± 15 % of dispersion from the mean value for the vertical velocity. In the riser part, it appears that the absolute values of the horizontal velocities are more than 1500 times lower than the vertical velocities. This observation confirms that the overall flow in the riser part describes an upward motion that is generated by the rising air bubbles, and that the suction velocity (0.04 mm/s) is too small to induce any horizontal flow near the membrane. Concerning the vertical flow, the average vertical velocity increased with the superficial gas velocity (and thus with air flowrate), and ranged between 0.03 and 0.2 when D_r was set to 7 mm, and between 0.01 and 0.2 when D_r was set to 15 mm. These results are in the same order of magnitude as previous studies on MBRs or ALMBRs, that was predictable and consistent according to works reporting the increase of the liquid velocity in ALRs with the superficial gas velocity [7,8,34,35]. In this study, when D_r was set to 7 mm, it was found that the average liquid velocity in the riser space could be correctly fitted by a power law function ($\overline{V_l} = a{U_{gr}}^b$) below a certain threshold value of the superficial gas velocity (here, comprised between 0.007 and 0.0085 $m.s^{-1}$) above which the liquid velocity reaches a plateau value (between 0.15 and 0.25 $m.s^{-1}$). When D_r was set to 15 mm, all the experimental data were well fitted by a power law function and no plateau value was reached in the investigated range of superficial gas velocity (from 0.0013 to 0.0044 $m.s^{-1}$). These results are in good agreement with a previous study investigating the hydrodynamics in a rectangular three-phase ALR with suspended polymeric particles in it [36].

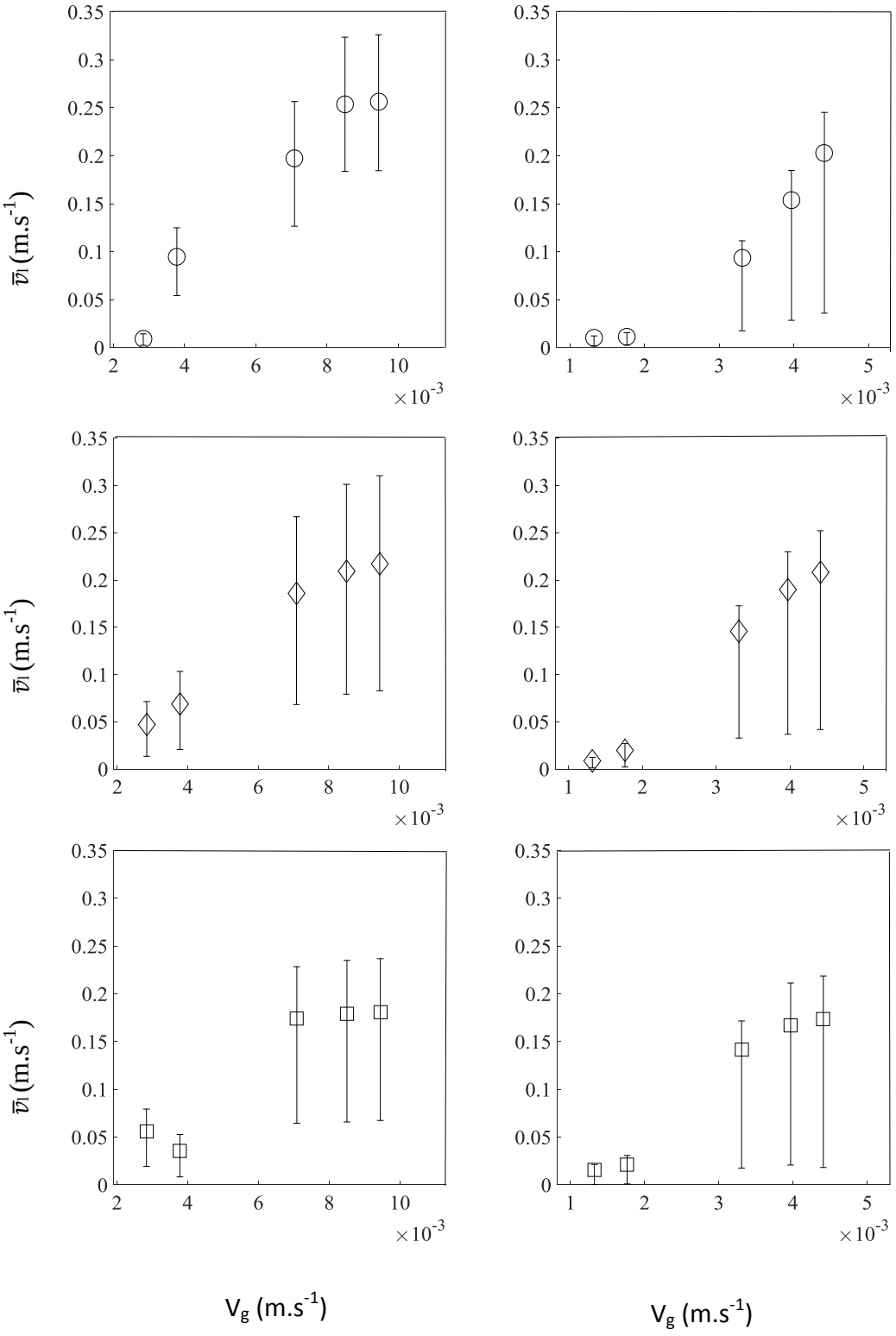


Figure 5: Average vertical liquid velocity $\overline{v}_l$ versus superficial gas velocity V_g in the riser at several height: ○: top; ◊: middle; □: bottom. Riser width: Left : 7mm ; right : 15 mm

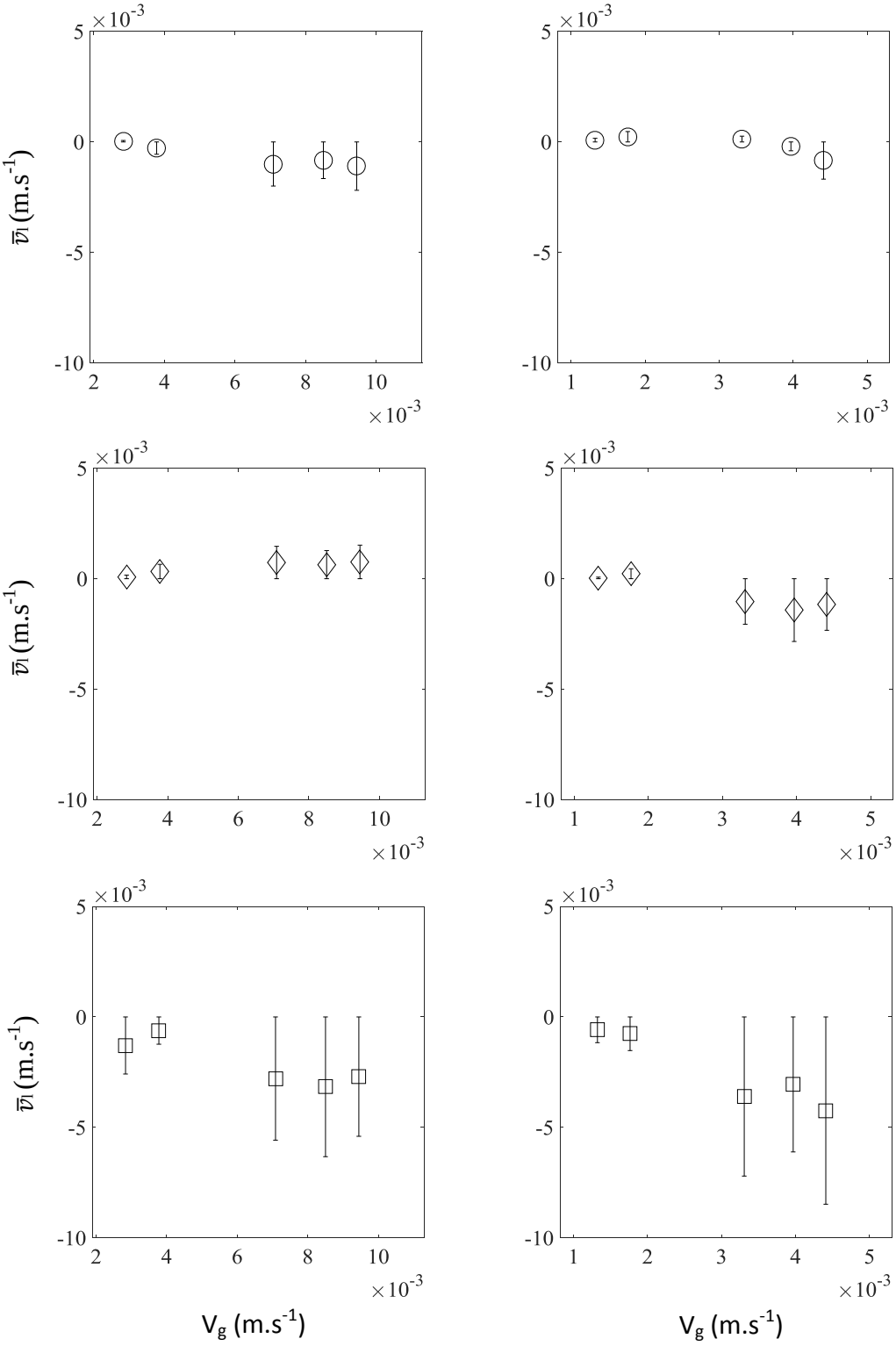


Figure 6: Average horizontal liquid velocity $\overline{v}_l$ versus superficial gas velocity Vg in the riser at several height: ○: top; ◊: middle; □: bottom. Riser width: Left : 7mm ; right : 15 mm

The liquid flow regime was characterized by calculating the Reynolds number (Re) based on the experimental average vertical liquid velocity ($\overline{V_l}$) in the riser part, according to the equation n°1, where D_h is the hydraulic diameter (m) (which corresponds in that case to $2D_r$), ρ is the water density (kg.m^{-3}) and μ is the water viscosity (Pa.s) at 20°C and 1 atm. The values of Re ranged between 130 and 3500 when the membrane and the baffle were 7 mm separated from each other. When this distance was set to 15 mm, the Re numbers ranged from 300 to 5000 for the different air flowrates (table 3).

$$Re = \frac{\rho D_h \overline{V_l}}{\mu} \qquad (1)$$

The horizontal profile of the experimental local value of the vertical velocity were plotted as well as the corresponding theoretical profiles, calculated with the average velocity, under the same conditions (figure 7). The comparison revealed that the experimental velocity profiles are closer to the theoretical laminar profiles when the riser width (D) is set to 7 mm. On the other hand, when the riser is 15 mm wide, the velocity profiles are closer to transitory/turbulent profiles. It is worth keeping in mind that the theoretical equations for laminar flow only concern the one phase flows, whereas this study deals with a two-phase flow, which can explain the differences that are still noticeable between the experimental and theoretical profiles. This observation indicates that the contribution of the gas phase to the two-phase flow may be less significant in confined spaces (in our case, when the riser is 7 mm wide).

Table 3: Reynolds number based on the average liquid vertical velocity in the riser part of the MBR.

	D_r= 7 mm					D_r = 15 mm				
SADm (Nm^3.h^{-1}.m^2)	**0.3**	**0.4**	**0.75**	**0.9**	**1**	**0.3**	**0.4**	**0.75**	**0.9**	**1**
Observation area										
I Top	127	1305	2729	3508	3546	296	332	2767	4553	6007
II Middle	652	954	2569	2895	3002	261	581	4314	5612	6156
III Bottom	777	492	2408	2479	2497	468	635	4197	4944	5140

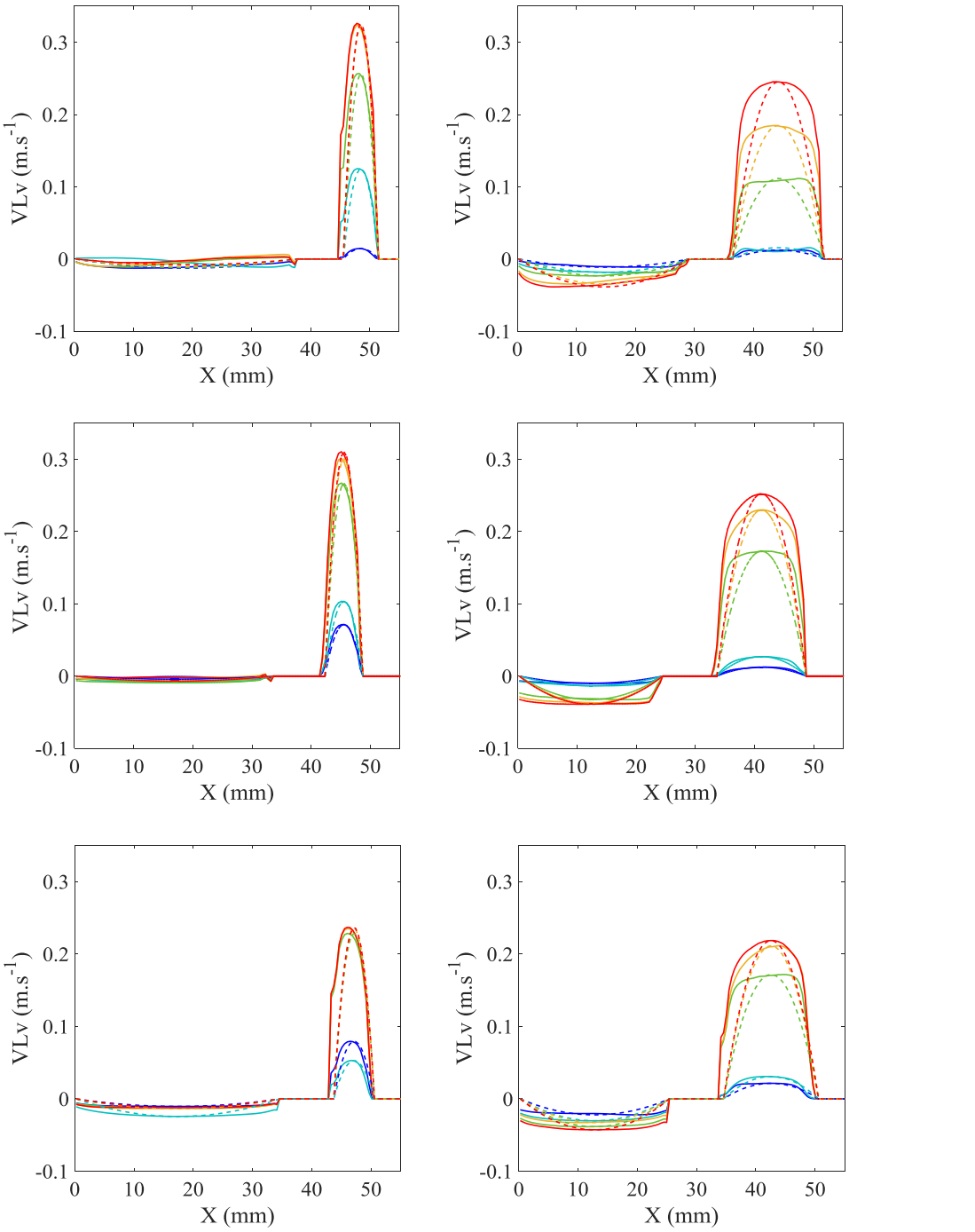


Figure 7: Experimental velocity profiles (solid line) and theoretical profiles (dotted line) in the two configurations of MBR (D = 7 mm (left) and D = 15 mm (right)) at several height, under different air flowrates SAD.

The membrane shear stress (τ) is defined as the viscosity force induced by the flow on the membrane surface. In the following, the membrane shear stress was obtained from the liquid cross-flow velocity and was calculated at a point of the membrane surface (figure 8), according to the equation n°2, where $V_y(x,y)$ is the vertical liquid velocity measured by the PIV technique at the local considered point (x,y).

$$\tau = \mu \left.\frac{\Delta V_y(x,y)}{\Delta x}\right|_{x_{membrane}\,,\,y_{middle}} \qquad (2)$$

The membrane shear stress is highly valuable information when studying aerated MBRs because it is strongly stated that the shear stress created by the bubbles circulation is involved in the biofouling reduction [8,9]. As a first approach an average membrane shear stress was determined and ranged approximately from 0.005 and 0.2 Pa, which appears lower than the average shear stress previously reported under similar conditions [10,11].

The local shear stress was determined for each condition and an example of the raw result is presented in figure 8. The profile obtained for the local membrane shear stress is a succession of sharp peaks which are induced by the passage of bubbles of which the streaks create a heightened velocity. The intensity of these peaks appears to be variable, and this may be correlated to the size of bubbles. Therefore it would be assumed that both the shear stress peak number and intensity can be key-factors for biofouling mitigation. Therefore, in order to take into account both of these factors at the same time, a peak size distribution has been determined for each condition. The peak size distribution is presented in terms of cumulative frequency of number of peaks versus the intensity of peaks (figure 8.c). As an example, when the MBR is run with a SADm of 0.9 $Nm^3.h.m^{-2}$, about 5 % of the shear stress peaks induced have at least an intensity of 0.5 Pa (figure 8.b and 8.c.). When the peak size distribution was comprehensively determined in the MBR under different air flowrates and at the different observation heights, the distribution curves tended to be shifted to the right when the airflow

rate increased, which indicates that intense membrane shear peaks are more likely to be induced at higher air flowrates (figure 9).

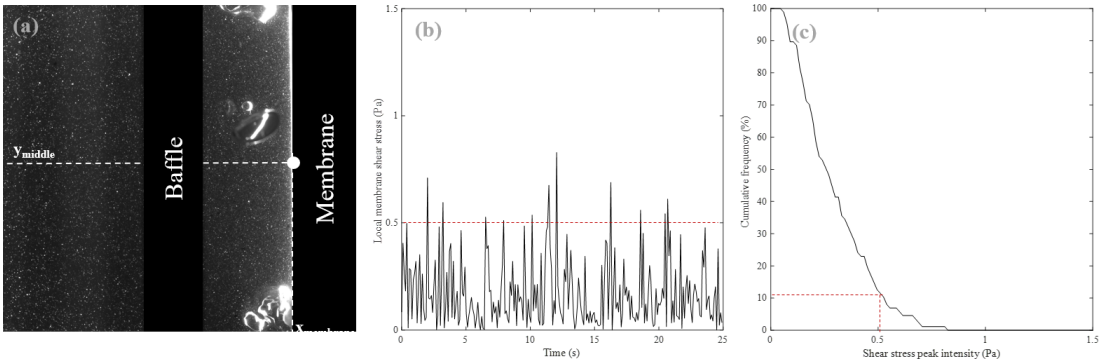


Figure 8 : (a) PIV image, (b) shear stress evolution at the local point ($x_{membrane}$,y_{middle}) and (c) its derived shear stress peak distribution, taken at the bottom of the reactor under a SADm of 0.9 $Nm^3.h^{-1}.m^2$ and with D_r = 15 mm.

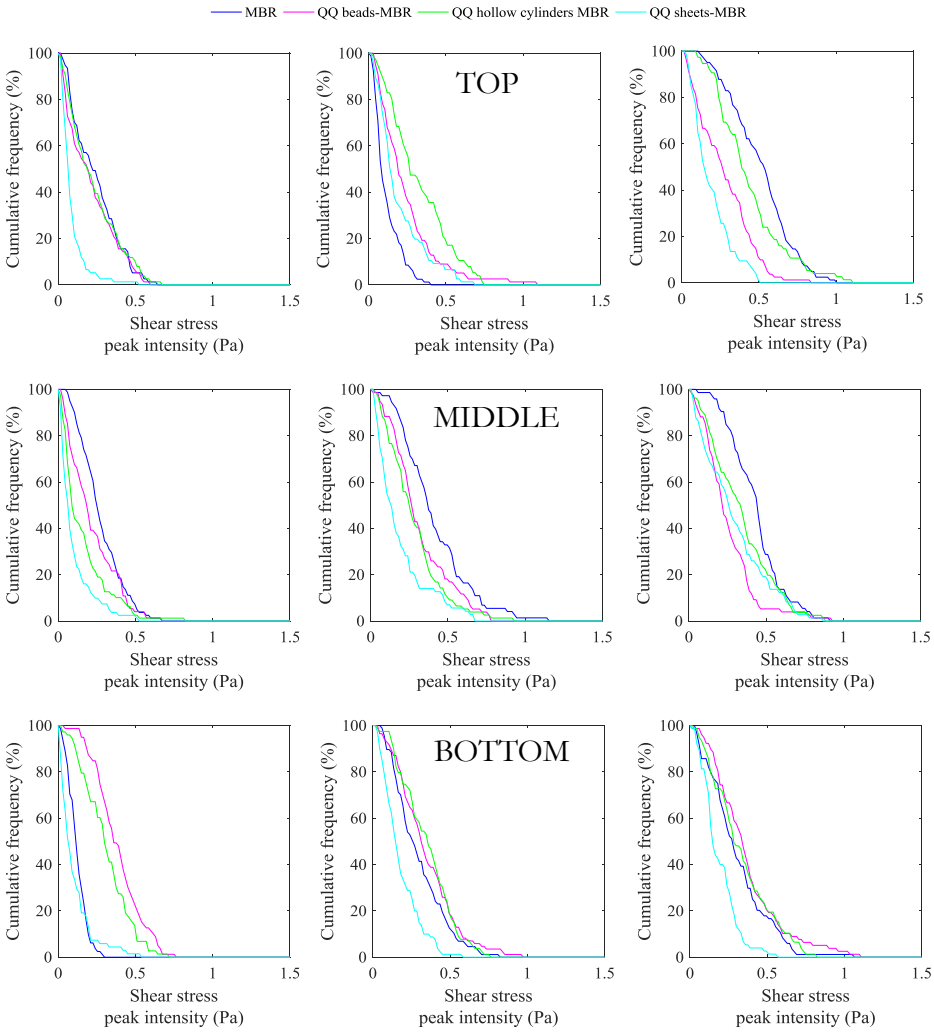


Figure 9: Local membrane shear stress distribution in the QQ-MBR at 0.45% under different air flowrates (SAD of 0.75 $Nm^3.h^{-1}.m^2$ (left), 0.9 $Nm^3.h^{-1}.m^2$ (middle) and 1 $Nm^3.h^{-1}.m^2$ (right)) and in different observation windows.

Therefore, the effect of the air flow rate and the resulting bubble size was analyzed since they could have a great impact on local shear stress. The bubble size was determined by processing images captured with the aforementioned visualization setup (figure 10), to measure the Circle Equivalent Diameter (CED) in terms of surface, under the different operating conditions. For each condition, the images of 10 bubbles were processed and the average bubble size was calculated over these 10 bubbles. The bubble size roughly ranged between 4.8 and 7.6 mm when D_r was set to 7 mm wide, and between 4.8 and 9.8 when D_r was 15 mm. To our best knowledge, few research studies focused on the characterization of air bubbles in similar geometrical configurations of ALMBRs. Also, the bubble size is strongly dependent on the sparger configuration and the superficial gas velocity. Hence, the comparison with other studies, as well as the validation of the order of magnitude, are in that case hard to achieve. The average bubble size for each condition is plotted versus the superficial gas velocity and presented in figure 11. No clear trend appears when observing the global shape of this plot, which means that the superficial gas velocity seems to have no noticeable influence on the bubble size. However, the comparison of the two columns of plots, reveals that the geometry of the ALMBR has greater influence, since it is possible to notice that the greatest riser width (also corresponding to the greatest ratio of the riser surface to the down-comer surface (Ar/Ad)) gives rise to bigger bubbles (figure 10). This result suggests that the geometrical characteristics of the ALMBR might have an influence on the bubble size, when the superficial gas velocity is kept constant. Concerning the error bars that represent the dispersion of results over the 10 bubbles that were characterized, they are bigger in the case where D_r is set to 15 mm. Thus, it seems that the greatest riser width (and thus the greatest (Ar/Ad) ratio) is most likely to give rise to more heterogeneous population of bubbles in terms of size. Finally, when comparing the results from the different observation windows, it appears that there is no significant modification of the bubbles behavior between

the bottom and the top of the ALMBR. It is worth mentioning though that these observations are to be taken carefully because they were deduced from the study of the reduced number of 10 bubbles, and a greater number of bubbles should be examined to draw statistically reliable conclusions. Also, the bubble size based on the CED is established on the hypothesis of spherical bubbles which can be far from their real shapes (figure 10). Thus, all these observations concerning the bubble size would need deeper research taking into account a greater number of bubbles as well as a better analysis of their shape.

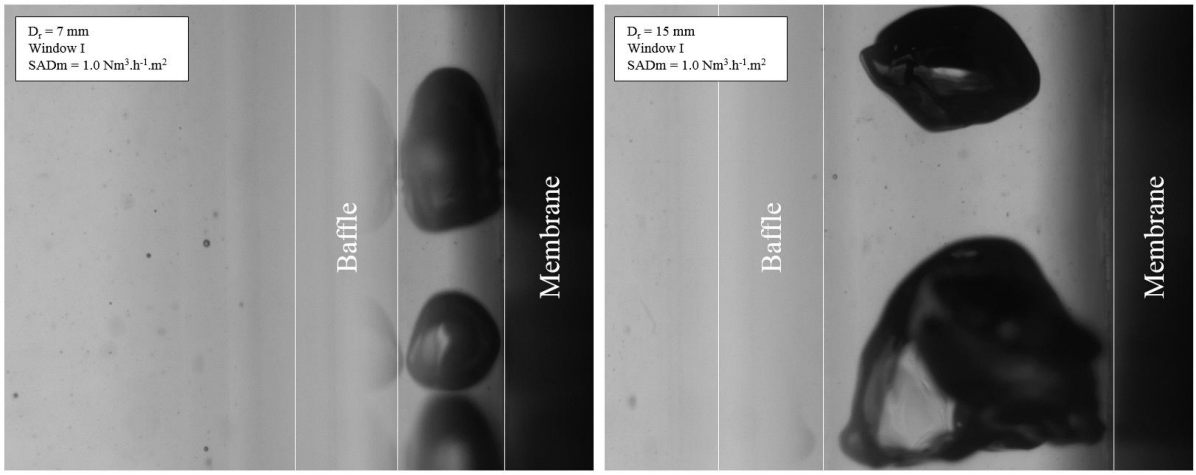


Figure 10: Example of images obtained with the direct visualization method.

However, the average bubble velocity was measured by processing the same images that were previously used for the bubble size determination. The bubble velocity was deduced by tracking the center of each bubble on a series of frames that were acquired at 200 Hz. Thus, the bubble velocity seems to be more reliable information than the bubble size, since no hypothesis is made on the bubble shape. The bubble velocity ranged approximately from 0.4 to 0.6 $m.s^{-1}$ when the distance between the membrane and the baffle was 7 mm; and from 0.35 to 0.65 $m.s^{-1}$ when the baffle was 15 mm away from the membrane. This order of magnitude is in accordance with a previous study in which the average bubble velocity was around 0.4 $m.s^{-1}$ for a population of bubbles among which 66 % had a size comprised between 3 and 5 mm. The average bubble velocity is higher than the average liquid velocity in the riser, for the

same conditions, which is consistent with the theory since the liquid flow is led by the bubbles rise.

3.2 Effect of particle addition

Three shape of particles at three concentrations were added in the water. A fluidization rate was defined as the percentage of solid media in suspension in relation to the total number of solid medias initially introduced in the reactor. The fluidization rate was visually measured by counting the suspended media on series of photographs for each experimental condition. A wide range of air flowrates was investigated in order to identify a potential optimal aeration intensity for the media fluidization. The first important result is that no fluidization was observed when D_r was set to 7 mm, probably because the space offered for the media to circulate is too narrow in that configuration. In contrast, when D_r was fixed to 15 mm, the solid media fluidization was observed (figure 11), for the three different shapes when they were introduced at three different volume fractions: 0.06, 0.10 and 0.45 % v/v. The error bars on figure 13 are due to the fact that the fluidization rate was measured on the basis of a relatively limited number of photographs that presented heterogeneous behaviors. Besides, the fluidization of solid media was observed to be a cyclic phenomenon, which means that, after a while, the solid media tend to settle and accumulate in dead zones of the reactor before being dragged again into the flow. It is possible to notice that, for all the shapes and volume fractions, the fluidization rate increases with the aeration, and that there is a critical airflow rate below which the particle tend to settle in the bottom of the reactor which is comprised between 0.4 and 0.5 $Nm^3.h^{-1}.m^{-2}$ in terms of SADm, (corresponding to 0.0018 and 0.0022 $m.s^{-1}$ in terms of superficial gas velocity). Concerning the volume fraction of media introduced, the greater volume fraction (0.45 % v/v) seems to induce lower fluidization rates in comparison to the other volume fractions. This latter observation can be attributed to a density effect referring to the fact that the motion of the solid media in the MBR is no longer

completely independent one from another because of their great number. Concerning the different shapes, the beads appear to reach lower fluidization rates than the hollow cylinders and sheets. This interesting result can be linked to the physical properties of the hollow cylinders and sheets, and more specifically to their surface which is more than 10 times greater than the beads surface (Table 2) and which probably offer them a better behavior in terms of hydrodynamics and extended lift force. Therefore, it appears that the MBR configuration of this study is more suitable for the fluidization of hollow cylinders and sheets than for beads. Thus, the physical washing effect of cylinders and sheets is expected to be more significant in this kind of ALMBR for the biofouling mitigation, which is in total accordance with a recent study reporting the enhanced physical washing effect of cylinders at the same concentration in a lab-scale MBR in comparison to beads (Lee et al., 2016).

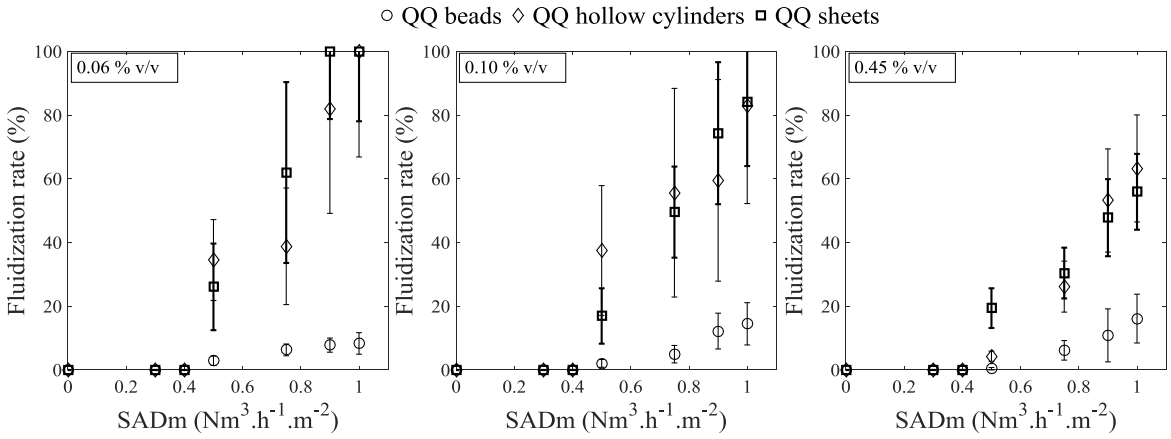


Figure 11: Fluidization rate of different shapes of solid media introduced at different volume fraction and measured under different air flowrates.

The average liquid velocity in the riser part was measured by the PIV method under different air flowrates when Solid media were added to the ALMBR at different volume fractions (0.06, 0.10 and 0.45 %v/v). The results are presented in figure 12. The introduction of solid media in suspension seems to have no major effect on the global trend followed by the average liquid velocity in the riser part (compared to figure 5). However, it appears that the

increase of the liquid velocity is less pronounced when sheets are added at high volume fractions (0.1 and 0.45 % v/v). As an example, the average liquid velocity reached with 0.45 % v/v of sheets is around 10 % lower than the liquid velocity in the simple ALMBR with no media in it, under the same conditions. This observation indicates that the sheets, which were previously found to have the lowest rising velocity, induce an overall slowdown of the liquid flow in the riser part, whereas the other shapes of Solid media (beads and hollow cylinders) have no significant influence on the liquid flow behavior. Similar results were obtained in previous studies where a slight decrease in the liquid velocity was caused by the introduction of suspended particles (Couvert et al., 2004).

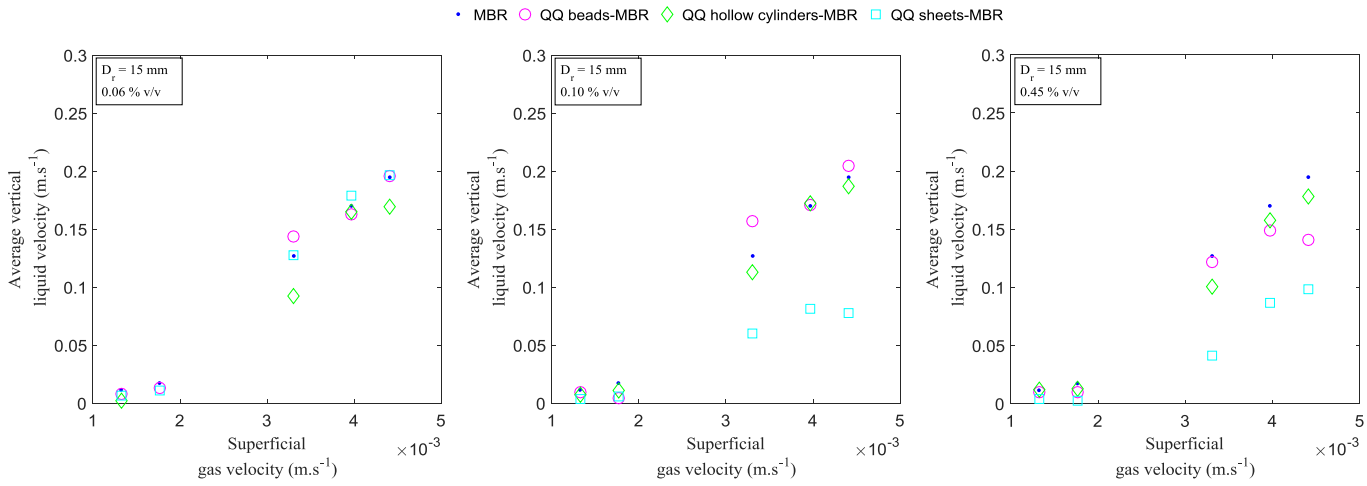


Figure 12: Evolution of the average horizontal liquid velocity with the superficial gas velocity in the riser part of the ALMBR, for different volume fractions of solid media. D_r = 15 mm.

As it was previously done, the Reynolds number was calculated using the average vertical liquid velocity in the riser when the Solid media were introduced under operating conditions that enhance their fluidization (volume fraction of 0.45 % v/v, D_r = 15 mm and under a high range of SADm). The results describe similar trend to those of the average liquid velocity, and again the sheets induce lower values compared to the other Solid media shapes, as well as, to the sole MBR. These findings indicate that the turbulence phenomena might be attenuated in presence of sheets.

The membrane shear stress in presence of suspended media in the MBR was studied in terms of shear stress peaks distribution for each solid media shape, as it was determined for the MBR alone. The results are gathered in figure 9, for three different air flowrates under which the Solid media fluidize significantly. As it was mentioned previously, the proportions of intense shear stress peaks increased in the MBR when the air flowrate increased. However, this trend is only maintained with the addition of hollow cylinders, whereas the beads and sheets induce random evolution of this same parameter. This observation indicates that, compared to the other shapes, the hollow cylinders might be less likely to impair the proper behavior of the MBR in terms of membrane shear stress created by the liquid flow, which is generated itself by the rising motion of bubbles. In addition, it is possible to notice that the peaks distribution obtained with the addition of solid sheets is almost always below the sole MBR, which indicate that they might reduce the intensity of the shear stress peaks, even though the sheets rise very close to the membrane but with the lowest rising velocity. Nevertheless, the global effect of media on the membrane shear stress is still hard to identify accurately based on this set of results. This probably comes from the difficulty to analyze the membrane shear stress which is deduced from the liquid phase characterization. Besides, the resolution of the PIV technique used for the liquid phase characterization is limited and cannot give information at less than 0.45 µm from the membrane surface, where local phenomena could still occur. The distribution method is a good way to take into account both the number and the intensity of instantaneous shear stress peaks in a local point, but some complementary information is still needed to precisely determine the effect of solid media on this parameter.

Conclusion

This work focused on the context of a recent and promising method (Quorum Quenching) for biofouling control in an AL-MBR, from a physical point of view and taking into account the hydrodynamics of such a system. The MBR was first characterized, and the results obtained were globally in good accordance with the literature, in terms of liquid velocity, membrane shear stress and bubbles behavior, which is important, considering the significant advantage of this configuration of reactors at the industrial scale. Secondly, the effect of the addition of solid media on the hydrodynamics was then investigated, firstly by studying their inherent behavior and then, by trying to identify their influence on the ALMBR parameters. The main results of this second part are gathered in table 4 under some specific operating conditions and distinguishing the three phases of the system.

- The observation of the solid phase section reveals that the greater is the air flowrate, the better is the fluidization of the solid media. The hollow cylinders seem to fluidize better than the beads, under the same conditions, which can probably be explained by their shape and surface. The velocities of the solid media while rising are in the same order of magnitude, however, the sheets appeared to be slower than the other shapes. Further research is needed though on these parts to know which position and velocity the more advantageous cases for Quorum Quenching would be to correctly mitigate biofouling.
- Concerning the liquid phase of the ALMBR, the hollow cylinders and beads induced no noticeable effect on any of the studied parameters, in the operating conditions of this study. However, under these conditions, all the results were in favor of the hypothesis that sheets (the slowest shape of media) seem to induce negative effect on the ALMBR, by slowing down the liquid velocity, reducing the turbulence phenomenon and the membrane shear stress.

- In contrast, the effect of media on the gas phase was found to be insignificant in the conditions of this study.

This work not only provides clues about application to MBRs, under a new perspective that was never approached before: hydrodynamics, but it also actually helps highlighting some gaps which could be subject to future research. Indeed, knowing that QQ is an efficient method based on the complex combination of several mechanisms (involving mass transfer, biochemical/enzymatic reactions, mechanical effect), it could of interest identifying which of these phenomena are the limiting ones and/or the governing ones.

Table 4: Quantitative properties of Solid media and their qualitative effect on hydrodynamic parameters at a volume fraction of 0.45 % v/v, with D_r = 15 mm and under variable air flowrates (SADm). (→ means no effect/↘ means decrease).

Parameter	beads-MBR	hollow cylinders-MBR	sheets-MBR
Solid phase			
Fluidization rate (%)	0 to 16	0 to 63	0 to 56
Liquid phase			
Average liquid velocity in the riser ($m.s^{-1}$)	→	→	↘
Flow regime (turbulence)	→	→	↘
Membrane shear stress	→	→	↘

References

(1) Bouayed, N.; Dietrich, N.; Lafforgue, C.; Lee, C.-H.; Guigui, C. Process-Oriented Review of Bacterial Quorum Quenching for Membrane Biofouling Mitigation in Membrane Bioreactors (MBRs). *Membranes* **2016**, *6* (4), 52. https://doi.org/10.3390/membranes6040052.

(2) Gander, M.; Jefferson, B.; Judd, S. Aerobic MBRs for Domestic Wastewater Treatment: A Review with Cost Considerations. *Separation and Purification Technology* **2000**, *18* (2), 119–130. https://doi.org/10.1016/S1383-5866(99)00056-8.

(3) Melin, T.; Jefferson, B.; Bixio, D.; Thoeye, C.; De Wilde, W.; De Koning, J.; van der Graaf, J.; Wintgens, T. Membrane Bioreactor Technology for Wastewater Treatment and Reuse. *Desalination* **2006**, *187* (1–3), 271–282. https://doi.org/10.1016/j.desal.2005.04.086.

(4) Brindle, K.; Stephenson, T. The Application of Membrane Biological Reactors for the Treatment of Wastewaters. *Biotechnol. Bioeng.* **1996**, *49* (6), 601–610. https://doi.org/10.1002/(SICI)1097-0290(19960320)49:6<601::AID-BIT1>3.0.CO;2-S.

(5) Lin, H.; Peng, W.; Zhang, M.; Chen, J.; Hong, H.; Zhang, Y. A Review on Anaerobic Membrane Bioreactors: Applications, Membrane Fouling and Future Perspectives. *Desalination* **2013**, *314*, 169–188. https://doi.org/10.1016/j.desal.2013.01.019.

(6) Meng, F.; Chae, S.-R.; Drews, A.; Kraume, M.; Shin, H.-S.; Yang, F. Recent Advances in Membrane Bioreactors (MBRs): Membrane Fouling and Membrane Material. *Water Research* **2009**, *43* (6), 1489–1512. https://doi.org/10.1016/j.watres.2008.12.044.

(7) Liu, R.; Huang, X.; Sun, Y. F.; Qian, Y. Hydrodynamic Effect on Sludge Accumulation over Membrane Surfaces in a Submerged Membrane Bioreactor. *Process Biochemistry* **2003**, *39* (2), 157–163. https://doi.org/10.1016/S0032-9592(03)00022-0.

(8) Liu, R.; Huang, X.; Wang, C.; Chen, L.; Qian, Y. Study on Hydraulic Characteristics in a Submerged Membrane Bioreactor Process. *Process Biochemistry* **2000**, *36* (3), 249–254. https://doi.org/10.1016/S0032-9592(00)00210-7.

(9) Prieske, H.; Drews, A.; Kraume, M. Prediction of the Circulation Velocity in a Membrane Bioreactor. *Desalination* **2008**, *231* (1), 219–226. https://doi.org/10.1016/j.desal.2007.12.010.

(10) Yan, X.; Wu, Q.; Sun, J.; Liang, P.; Zhang, X.; Xiao, K.; Huang, X. Hydrodynamic Optimization of Membrane Bioreactor by Horizontal Geometry Modification Using Computational Fluid Dynamics. *Bioresource Technology* **2016**, *200*, 328–334. https://doi.org/10.1016/j.biortech.2015.10.050.

(11) Yan, X.; Xiao, K.; Liang, S.; Lei, T.; Liang, P.; Xue, T.; Yu, K.; Guan, J.; Huang, X. Hydraulic Optimization of Membrane Bioreactor via Baffle Modification Using Computational Fluid Dynamics. *Bioresource Technology* **2015**, *175*, 633–637. https://doi.org/10.1016/j.biortech.2014.10.133.

(12) Oh, H.-S.; Yeon, K.-M.; Yang, C.-S.; Kim, S.-R.; Lee, C.-H.; Park, S. Y.; Han, J. Y.; Lee, J.-K. Control of Membrane Biofouling in MBR for Wastewater Treatment by Quorum Quenching Bacteria Encapsulated in Microporous Membrane. *Environ. Sci. Technol.* **2012**, *46* (9), 4877–4884. https://doi.org/10.1021/es204312u.

(13) Siddiqui, M. F.; Sakinah, M.; Singh, L.; Zularisam, A. W. Targeting N-Acyl-Homoserine-Lactones to Mitigate Membrane Biofouling Based on Quorum Sensing Using a Biofouling Reducer. *Journal of Biotechnology* **2012**, *161* (3), 190–197. https://doi.org/10.1016/j.jbiotec.2012.06.029.

(14) Siddiqui, M. F.; Rzechowicz, M.; Harvey, W.; Zularisam, A. W.; Anthony, G. F. Quorum Sensing Based Membrane Biofouling Control for Water Treatment: A

Review. *Journal of Water Process Engineering* **2015**, *7*, 112–122. https://doi.org/10.1016/j.jwpe.2015.06.003.

(15) Köse-Mutlu, B.; Ergön-Can, T.; Koyuncu, I.; Lee, C.-H.; Köse-Mutlu, B.; Ergön-Can, T.; Koyuncu, I.; Lee, C.-H. Quorum Quenching for Effective Control of Biofouling in Membrane Bioreactor: A Comprehensive Review of Approaches, Applications, and Challenges. *Environmental Engineering Research* **2019**, *24* (4), 543–558. https://doi.org/10.4491/eer.2018.380.

(16) Lee, S.; Lee, S. H.; Lee, K.; Kwon, H.; Nahm, C. H.; Lee, C.-H.; Park, P.-K.; Choo, K.-H.; Lee, J.-K.; Oh, H.-S. Effect of the Shape and Size of Quorum Quenching Media on Biofouling Control in Membrane Bioreactors for Wastewater Treatment. *J. Microbiol. Biotechnol.* **2016**. https://doi.org/10.4014/jmb.1605.05021.

(17) Lee, S. H.; Lee, S.; Lee, K.; Nahm, C. H.; Kwon, H.; Oh, H.-S.; Won, Y.-J.; Choo, K.-H.; Lee, C.-H.; Park, P.-K. More Efficient Media Design for Enhanced Biofouling Control in a Membrane Bioreactor: Quorum Quenching Bacteria Entrapping Hollow Cylinder. *Environ. Sci. Technol.* **2016**, *50* (16), 8596–8604. https://doi.org/10.1021/acs.est.6b01221.

(18) Nahm, C. H.; Choi, D.-C.; Kwon, H.; Lee, S.; Lee, S. H.; Lee, K.; Choo, K.-H.; Lee, J.-K.; Lee, C.-H.; Park, P.-K. Application of Quorum Quenching Bacteria Entrapping Sheets to Enhance Biofouling Control in a Membrane Bioreactor with a Hollow Fiber Module. *Journal of Membrane Science* **2017**, *526*, 264–271. https://doi.org/10.1016/j.memsci.2016.12.046.

(19) Kim, S.-R.; Lee, K.-B.; Kim, J.-E.; Won, Y.-J.; Yeon, K.-M.; Lee, C.-H.; Lim, D.-J. Macroencapsulation of Quorum Quenching Bacteria by Polymeric Membrane Layer and Its Application to MBR for Biofouling Control. *Journal of Membrane Science* **2015**, *473*, 109–117. https://doi.org/10.1016/j.memsci.2014.09.009.

(20) Kim, S.-R.; Oh, H.-S.; Jo, S.-J.; Yeon, K.-M.; Lee, C.-H.; Lim, D.-J.; Lee, C.-H.; Lee, J.-K. Biofouling Control with Bead-Entrapped Quorum Quenching Bacteria in Membrane Bioreactors: Physical and Biological Effects. *Environ. Sci. Technol.* **2013**, *47* (2), 836–842. https://doi.org/10.1021/es303995s.

(21) Köse-Mutlu, B.; Ergön-Can, T.; Koyuncu, İ.; Lee, C.-H. Quorum Quenching MBR Operations for Biofouling Control under Different Operation Conditions and Using Different Immobilization Media. *Desalination and Water Treatment* **2015**, *0* (0), 1–11. https://doi.org/10.1080/19443994.2015.1086899.

(22) Lee, S.; Park, S.-K.; Kwon, H.; Lee, S. H.; Lee, K.; Nahm, C. H.; Jo, S. J.; Oh, H.-S.; Park, P.-K.; Choo, K.-H.; et al. Crossing the Border between Laboratory and Field: Bacterial Quorum Quenching for Anti-Biofouling Strategy in an MBR. *Environ. Sci. Technol.* **2016**. https://doi.org/10.1021/acs.est.5b04795.

(23) Maqbool, T.; Khan, S. J.; Waheed, H.; Lee, C.-H.; Hashmi, I.; Iqbal, H. Membrane Biofouling Retardation and Improved Sludge Characteristics Using Quorum Quenching Bacteria in Submerged Membrane Bioreactor. *Journal of Membrane Science* **2015**, *483*, 75–83. https://doi.org/10.1016/j.memsci.2015.02.011.

(24) Teychene, B.; Guigui, C.; Cabassud, C. Engineering of an MBR Supernatant Fouling Layer by Fine Particles Addition: A Possible Way to Control Cake Compressibility. *Water Research* **2011**, *45* (5), 2060–2072. https://doi.org/10.1016/j.watres.2010.12.018.

(25) Wu, B.; Zamani, F.; Lim, W.; Liao, D.; Wang, Y.; Liu, Y.; Chew, J. W.; Fane, A. G. Effect of Mechanical Scouring by Granular Activated Carbon (GAC) on Membrane Fouling Mitigation. *Desalination* **2017**, *403*, 80–87. https://doi.org/10.1016/j.desal.2015.12.003.

(26) Aslam, M.; Charfi, A.; Lesage, G.; Heran, M.; Kim, J. Membrane Bioreactors for Wastewater Treatment: A Review of Mechanical Cleaning by Scouring Agents to

Control Membrane Fouling. *Chemical Engineering Journal* **2017**, *307*, 897–913. https://doi.org/10.1016/j.cej.2016.08.144.

(27) Lesage, N.; Sperandio, M.; Cabassud, C. Study of a Hybrid Process: Adsorption on Activated Carbon/Membrane Bioreactor for the Treatment of an Industrial Wastewater. *Chemical Engineering and Processing: Process Intensification* **2008**, *47* (3), 303–307. https://doi.org/10.1016/j.cep.2007.01.021.

(28) Xu, F.; Jimenez, M.; Dietrich, N.; Hébrard, G. Fast Determination of Gas-Liquid Diffusion Coefficient by an Innovative Double Approach. *Chemical Engineering Science* **2017**, *170* (Supplement C), 68–76. https://doi.org/10.1016/j.ces.2017.02.043.

(29) Dietrich, N.; Hebrard, G. Visualisation of Gas-Liquid Mass Transfer around a Rising Bubble in a Quiescent Liquid Using an Oxygen Sensitive Dye. *Heat Mass Transfer* **2018**, 1–9. https://doi.org/10.1007/s00231-018-2297-3.

(30) Xu, F.; Cockx, A.; Hébrard, G.; Dietrich, N. Mass Transfer and Diffusion of a Single Bubble Rising in Polymer Solutions. *Ind. Eng. Chem. Res.* **2018**, *57* (44), 15181–15194. https://doi.org/10.1021/acs.iecr.8b03617.

(31) Xu, F.; Hébrard, G.; Dietrich, N. Comparison of Three Different Techniques for Gas-Liquid Mass Transfer Visualization. *International Journal of Heat and Mass Transfer* **2020**, *150*, 119261. https://doi.org/10.1016/j.ijheatmasstransfer.2019.119261.

(32) Xie, X.; Le Men, C.; Dietrich, N.; Schmitz, P.; Fillaudeau, L. Local Hydrodynamic Investigation by PIV and CFD within a Dynamic Filtration Unit under Laminar Flow. *Separation and Purification Technology* **2017**. https://doi.org/10.1016/j.seppur.2017.04.009.

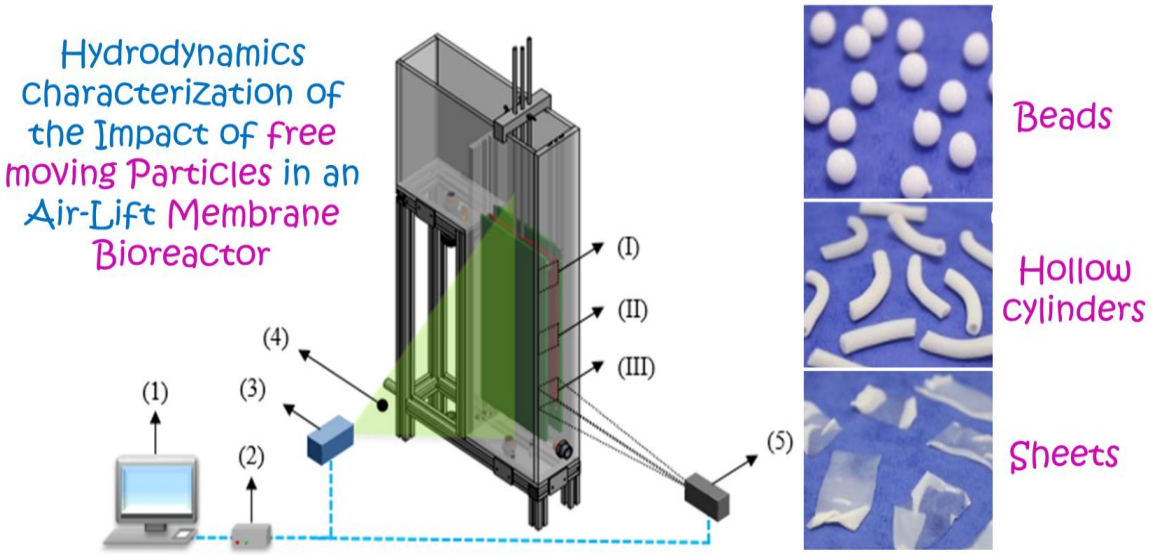
(33) Xie, X.; Dietrich, N.; Fillaudeau, L.; Le Men, C.; Schmitz, P.; Liné, A. Local Hydrodynamics Investigation within a Dynamic Filtration Unit under Laminar Flow. *Chemical Engineering Research and Design* **2018**, *132*, 954–965. https://doi.org/10.1016/j.cherd.2018.02.018.

(34) Bello, R. A.; Robinson, C. W.; Moo-Young, M. Liquid Circulation and Mixing Characteristics of Airlift Contactors. *Can. J. Chem. Eng.* **1984**, *62* (5), 573–577. https://doi.org/10.1002/cjce.5450620501.

(35) Couvert, A.; Bastoul, D.; Roustan, M.; Line, A.; Chatellier, P. Prediction of Liquid Velocity and Gas Hold-up in Rectangular Air-Lift Reactors of Different Scales. *Chemical Engineering and Processing: Process Intensification* **2001**, *40* (2), 113–119. https://doi.org/10.1016/S0255-2701(00)00130-6.

(36) Couvert, A.; Bastoul, D.; Roustan, M.; Chatellier, P. Hydrodynamic and Mass Transfer Study in a Rectangular Three-Phase Air-Lift Loop Reactor. *Chemical Engineering and Processing: Process Intensification* **2004**, *43* (11), 1381–1387. https://doi.org/10.1016/j.cep.2003.06.001.

630 **Table of content**



631